







Ozone responses in *Arabidopsis*: beyond stomatal conductance

Luis O. Morales ^{1,2} Alexey Shapiguzov ^{1,3} Omid Safronov ¹ Johanna Leppälä,^{1,4}
Lauri Vaahtera ^{1,5} Dmitry Yarmolinsky ⁶ Hannes Kollist ⁶ and Mikael Brosché,^{1,*†}

- 1 Organismal and Evolutionary Biology Research Programme, Faculty of Biological and Environmental Sciences, Viikki Plant Science Centre, University of Helsinki, FIN-00014 Helsinki, Finland
- 2 School of Science & Technology, The Life Science Center-Biology, Örebro University, SE-70182 Örebro, Sweden
- 3 Institute of Plant Physiology, Russian Academy of Sciences, 127276 Moscow, Russia
- 4 Department of Ecology and Environmental Sciences, Umeå University, 90187 Umeå, Sweden
- 5 Department of Biology, Norwegian University of Science and Technology (NTNU), NO-7491 Trondheim, Norway
- 6 Institute of Technology, University of Tartu, 50411 Tartu, Estonia

*Author for communication: mikael.brosche@helsinki.fi

†Senior author.

L.O.M. and M.B. conceived the research; L.O.M., A.S., J.L., D.Y., and L.V. performed experiments; L.O.M., A.S., D.Y., O.S., and H.K. performed data analysis; L.O.M. and M.B. wrote the article with contributions of all the authors.

The author responsible for distribution of materials integral to the findings presented in this article in accordance with the policy described in the Instructions for Authors (<https://academic.oup.com/plphys/pages/general-instructions>) is: Mikael Brosché (mikael.brosche@helsinki.fi).

Abstract

Tropospheric ozone (O₃) is a major air pollutant that decreases yield of important crops worldwide. Despite long-lasting research of its negative effects on plants, there are many gaps in our knowledge on how plants respond to O₃. In this study, we used natural variation in the model plant *Arabidopsis* (*Arabidopsis thaliana*) to characterize molecular and physiological mechanisms underlying O₃ sensitivity. A key parameter in models for O₃ damage is stomatal uptake. Here we show that the extent of O₃ damage in the sensitive *Arabidopsis* accession Shahdara (Sha) does not correspond with O₃ uptake, pointing toward stomata-independent mechanisms for the development of O₃ damage. We compared tolerant (Col-0) versus sensitive accessions (Sha, Cvi-0) in assays related to photosynthesis, cell death, antioxidants, and transcriptional regulation. Acute O₃ exposure increased cell death, development of lesions in the leaves, and decreased photosynthesis in sensitive accessions. In both Sha and Cvi-0, O₃-induced lesions were associated with decreased maximal chlorophyll fluorescence and low quantum yield of electron transfer from Photosystem II to plastoquinone. However, O₃-induced repression of photosynthesis in these two O₃-sensitive accessions developed in different ways. We demonstrate that O₃ sensitivity in *Arabidopsis* is influenced by genetic diversity given that Sha and Cvi-0 developed accession-specific transcriptional responses to O₃. Our findings advance the understanding of plant responses to O₃ and set a framework for future studies to characterize molecular and physiological mechanisms allowing plants to respond to high O₃ levels in the atmosphere as a result of high air pollution and climate change.

Introduction

Plants are continuously exposed to adverse environmental conditions that impair growth and fitness (Suzuki et al., 2014). Ozone (O₃) is a phytotoxic air pollutant that reduces the yield of important crops worldwide (Ainsworth et al., 2012). O₃ enters the plant through stomata and in the apoplast it breaks down into reactive oxygen species (ROS), such as superoxide (O₂⁻) and hydrogen peroxide (H₂O₂; Ainsworth, 2017; Waszczak et al., 2018). Depending on the O₃ concentration, sensitive plant species activate cell death programs leading to the development of lesions (Brosché et al., 2010; Langebartels et al., 2002). O₃ and most abiotic and biotic stresses increase the formation of ROS with potentially deleterious toxic effects on DNA, proteins, lipids, and carbohydrates. However, ROS are not merely damaging molecules, as they also initiate signaling events that help plants acclimate to stress (Jaspers and Kangasjärvi, 2010; Waszczak et al., 2018).

Plants actively produce ROS as signaling molecules to regulate developmental and defense programs (Huang et al., 2019). One of the earliest detectable responses in defense against pathogens and abiotic stresses is increased apoplastic ROS production (often referred to a ROS burst; Shimada et al., 2003; Choudhury et al., 2017; Qi et al., 2017). As treatments with O₃ allow a controlled delivery of apoplastic ROS to plants without further manipulation, O₃ is a very useful tool to study general mechanisms of ROS signaling and its role in cell death, defense signaling, and regulation of gene expression (Vainonen and Kangasjärvi, 2015; Xu et al., 2015a). Apoplastic ROS signaling triggered by O₃ induces large scale changes in gene expression and metabolic profiles (Blomster et al., 2011; Xu et al., 2015a). However, mechanistic understanding of how ROS regulate gene expression is very limited as only few specific components of ROS signaling have been deciphered in plants. Overall, studies with O₃ can fulfill two goals at the same time: (1) How do plants protect themselves against this air pollutant? and (2) How do plants use ROS to regulate defense signaling?

The large genetic variation between naturally occurring populations/accessions of *Arabidopsis* (*Arabidopsis thaliana*) provides a unique resource to study the complex mechanisms underlying stress tolerance. *Arabidopsis* accessions display different O₃ sensitivity which is largely explained by stomatal conductance regulating O₃ uptake and cell death in O₃ sensitive genotypes (Brosché et al., 2010; Xu et al., 2015b). The O₃ sensitive accession from the Cape Verde islands Cvi-0 (hereafter, Cvi) has constitutively high stomatal conductance and increased O₃ uptake caused by impaired function of MITOGEN-ACTIVATED PROTEIN KINASE12 (Brosché et al., 2010; Jakobson et al., 2016). Mutant analysis in *Arabidopsis* showed that O₃ activates an abscisic acid (ABA) signaling pathway that ultimately leads to stomatal closure through SLOW ANION CHANNEL1 (Merilo et al., 2013). In addition, several *Arabidopsis* mutants with increased stomatal conductance display O₃ sensitivity (Overmyer et al., 2008; Hörak et al., 2016; Sierla et al., 2018). However, O₃ responses in *Arabidopsis* are very complex and clearly involve other physiological functions

in addition to stomatal opening (Overmyer et al., 2008). Thus, further characterization of O₃ responses in sensitive *Arabidopsis* accessions is needed to unravel genetic and molecular mechanisms underlying O₃ sensitivity in plants.

Shahdara (Sha), an *Arabidopsis* accession from Tajikistan in Central Asia was identified as highly O₃ sensitive (Brosché et al., 2010). Sha is also tolerant to drought and salt stress, has low chlorophyll content, and low levels of ABA (Bouchabka et al., 2008; Sharma et al., 2013; Szymańska et al., 2015; Kalladan et al., 2019). Thus, given its O₃ sensitivity and altered stress responses, Sha is a good candidate to reveal mechanisms of plant O₃ responses.

A consistent physiological O₃ response across many plant species and O₃ doses is a decreased rate of photosynthesis and reduced expression of photosynthesis-related genes (Fiscus et al., 2005; Wittig et al., 2007; Kontunen-Soppela et al., 2010a; Vainonen and Kangasjärvi, 2015). High O₃ concentrations reduce the abundance of photosynthetic proteins and pigments, which decrease photosynthetic rates, growth, and biomass production (Ainsworth et al., 2012; Ainsworth, 2017). The use of chlorophyll *a* fluorescence (ChlF) measurements has allowed the assessment of photosynthesis under different stress conditions including O₃ (Baker, 2008; Bussotti et al., 2011). Measured ChlF parameters in several tree species indicated that O₃ can affect activities of both Photosystems II and I (PSII and PSI, accordingly; Bussotti et al., 2011). However, in most such studies, the spatiotemporal resolution of ChlF analyses was insufficient to gain insight into kinetics and mechanisms of O₃-induced damage to photosynthesis.

Transcriptional reprogramming is an early response in plants exposed to abiotic and biotic stresses (Atkinson and Erwin, 2012). Transcriptional responses to O₃ have been studied in several species: *Arabidopsis* (Blomster et al., 2011; Brosché et al., 2014; Xu et al., 2015a), rice (*Oryza sativa* L; Ashrafuzzaman et al., 2018), silver birch (*Betula pendula* Roth; Kontunen-Soppela et al., 2010b), and *Medicago* (*Medicago truncatula*; Iyer et al., 2013). Mutant analysis in *Arabidopsis* identified regulators of O₃-induced transcriptional responses, including the plant stress hormones ethylene, salicylic acid (SA) and jasmonic acid (Xu et al., 2015a). Furthermore, cell death induced by O₃ in *Arabidopsis* requires altered transcriptional programs (Overmyer et al., 2005). Plants use a large number of transcription factors (TFs) to regulate changes in gene expression (Khan et al., 2018; Tian et al., 2019). In relation to O₃, TFs from the families ETHYLENE RESPONSE FACTORS (ERF), TGA, and WRKY regulate some aspects of the O₃ response (Xu et al., 2015a). However, several more unidentified TFs are likely to be involved (Xu et al., 2015a).

In this study, we characterized molecular and physiological mechanisms underlying O₃ sensitivity and ROS signaling in *Arabidopsis*. To that end, we designed a series of experiments with *Arabidopsis* accessions having different O₃ sensitivities including Col-0 (hereafter, Col) as O₃ tolerant, and Sha and Cvi as O₃ sensitive. O₃ sensitivity was characterized by measuring stomatal conductance, photosynthetic

performance, abundance of antioxidants, and changes in gene expression.

Results

O₃ sensitivity in Sha is associated with increased cell death

O₃ sensitivity in Sha was first characterized by measuring cell death under various O₃ doses. Exposure to 350 nL L⁻¹ of O₃ for 6 h induced a significantly higher percentage of cell death in Sha than in Col ($P < 0.001$; Figure 1A). Cell death in Sha also corresponded to increased lesion area in the leaves as compared with Col (Figure 1B). Exposure to 200 and 250 nL L⁻¹ of O₃ for 6 h also increased cell death and lesion formation in Sha leaves as compared with Col ($P < 0.05$; Supplemental Figure S1). Previous research indicated that Arabidopsis mutants with lower concentration of the antioxidant ascorbic acid (AA) are O₃ sensitive (Conklin et al., 2000). AA measurements showed that Sha contained approximately 20% lower levels of AA and dehydroascorbic acid than Col both under CA and O₃ 350 nL L⁻¹ for 2 h (Supplemental Figure S2).

O₃ sensitivity in Sha was not linked to high stomatal conductance

Several O₃-sensitive Arabidopsis accessions display high stomatal conductance and high O₃ uptake during the first 30 min of acute O₃ exposure, traits that are positively correlated with O₃-induced cell death (Brosché et al., 2010). To assess the relationship of gas exchange parameters with the O₃ sensitivity in Sha, 3 weeks old plants were exposed to O₃ and stomatal conductance, rate of O₃ uptake and cumulative O₃ dose were measured during 4 h (Figure 2, A and B). Col and Sha had similar stomatal conductance in control conditions (Figure 2A, Supplemental Figure S3). In response

to O₃, Col had a rapid drop in stomatal conductance (referred to as rapid transient decrease), followed by reopening of stomata and finally, a sustained decrease in stomatal conductance (Vahisalu et al., 2010). After O₃ exposure, both Col and Sha showed the same rapid decrease in stomatal conductance (Figure 2A; Supplemental Figure S3A); however, while Col recovered its stomatal conductance, this response was much weaker in Sha. Although the stomatal uptake rate was slightly different in Col and Sha after 16 and 32 min of O₃ onset, both genotypes received the same cumulative O₃ doses during the first 48 min of O₃ exposure (Figure 2B; Supplemental Figure S3, B and C). In the continued O₃ exposure, stomatal conductance in Sha eventually dropped to very low values, while Col still maintained ~30% of stomatal conductance. Consequently, Sha plants had lower O₃ uptake and lower total cumulative O₃ dose as compared with Col plants (Figure 2B; Supplemental Figure S3, B and C). This indicates that O₃ sensitivity in Sha is regulated through stomata-independent mechanisms.

Photosynthesis is severely impaired in Sha by O₃

To assess the direct O₃ effects on photosynthetic activity in Sha, we first measured net photosynthesis using gas exchange in three weeks old plants exposed to O₃ for 4 h. Despite considerably reduced stomatal conductance during O₃ exposure (Figure 2A), Col maintained its photosynthetic activity. As plants for gas exchange were grown in relatively low light conditions (150 μE), decreased CO₂ uptake through reduced stomatal apertures was probably not a limitation for photosynthesis (Tanaka et al., 2013). In contrast to Col, net photosynthesis started to progressively decline in Sha approximately 2 h after the onset of the O₃ treatment (Figure 2C; Supplemental Figure S3D). Importantly, Col displayed higher net photosynthesis than Sha at approximately

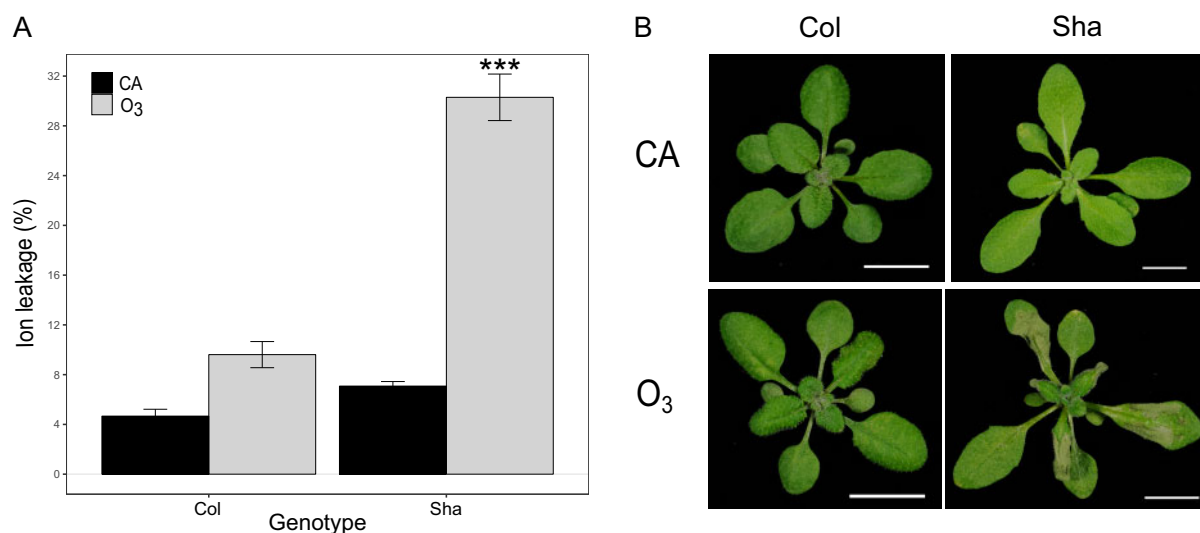


Figure 1 O₃ response in Col and Sha plants exposed to 350 nL L⁻¹ of O₃ during 6 h. A, Cell death measurements with ion leakage in CA control and O₃ treated plants. Mean of four independent experiments \pm SE is shown ($n = 32$). The asterisks denote significant differences ($P < 0.001$) between O₃-induced cell death in Col and Sha assessed with the function fit.contrast from gmodels 2.18.1 (Warnes et al., 2018). B, Representative pictures taken 24 h after the O₃ exposure was finished (scale bar 1cm).

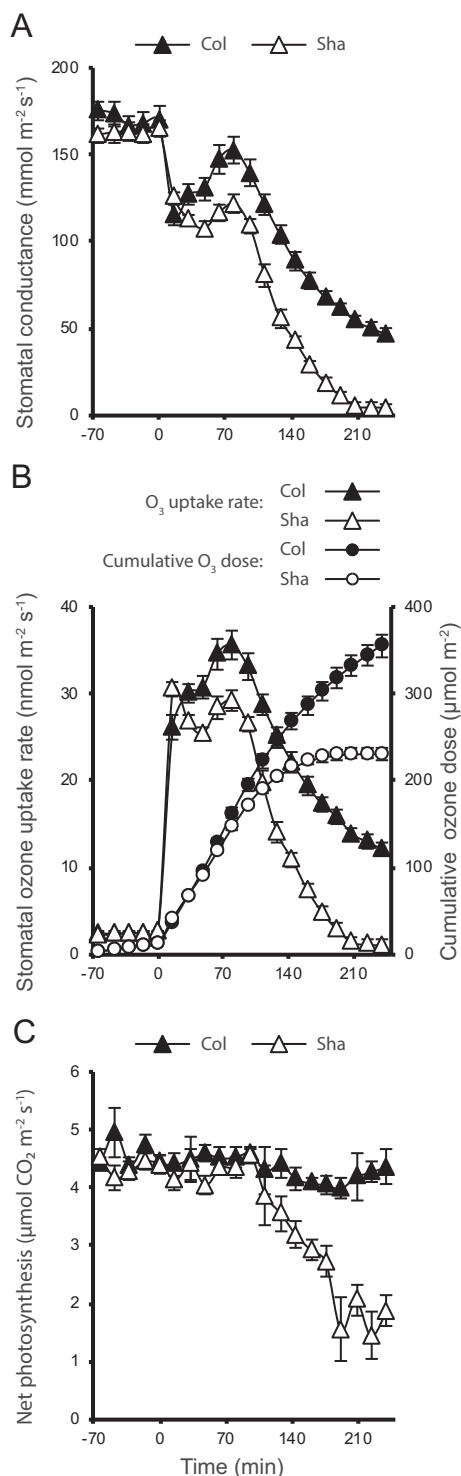


Figure 2 Gas exchange and photosynthetic response in Col and Sha subjected to O_3 treatments. Time course of (A) stomatal conductance, (B) O_3 uptake, and (C) and photosynthetic response measured in 3.5-week-old plants exposed to $423 \pm 8.2 \text{ nL L}^{-1} O_3$ during 4 h. Mean of three independent experiments \pm SE is shown ($n = 12$).

the same values of stomatal conductance (256 min after O_3 onset for Col and 144 min for Sha; Figure 2, A and C). This suggested that the decline of photosynthesis in Sha was not related to stomatal function.

In relation to O_3 , photosynthetic traits are usually measured in the whole plant or organ (i.e. leaf) after the specified time of exposure. However, by increasing the spatiotemporal resolution of the measurements, new insights can be gained into what aspects of photosynthesis are the O_3 targets. We performed real-time monitoring of the O_3 -induced changes of photosynthesis using Pulse Amplitude Modulated (PAM) ChlF imaging. In addition to Sha, we included Cvi as a second O_3 -sensitive accession and compared photosynthetic parameters with those in the O_3 -tolerant Col. Two-week-old plants were exposed to O_3 and ChlF was monitored from the onset of the O_3 treatment. Against the background actinic light, saturating light pulses were given every 10 min to image maximal fluorescence, F_m' . After 1.5–2 h of O_3 exposure, local lesions developed in Sha leaves. These lesions were originally only visible as depressions of F_m' (Figure 3). Notably, the lesions developed in a short time window of 10 min or less, and at the early stage did not coincide with changes in basal light-adapted fluorescence (F_s ; white arrows in Figure 3). Quantification of the effective quantum yield of PSII photochemistry (ϕPSII) revealed difference in photosynthetic electron transfer between the three accessions. No change of ϕPSII was observed in Col; however, massive drop of ϕPSII occurred in rosettes of Cvi, while in Sha ϕPSII originally decreased only within the local lesions (Figure 3C). During the following hour, the Sha lesions expanded, ultimately leading to leaf tissue collapse. This later stage was accompanied by rising F_s , the characteristic feature of disassembling photosynthetic apparatus. In Sha, rising F_s was accompanied with temporary partial recovery of F_m' , this effect was much less pronounced in Cvi (Figure 3B).

Quenching of F_m' is referred to as nonphotochemical quenching (NPQ). The two main constituents of NPQ are the energy-dependent quenching (qE) associated with acidification of thylakoids and photoinhibitory quenching (qI) caused by damage to PSII (Baker, 2008). The difference between qE and qI can be revealed by dark adaptation. The qE component dissipates within 10–30 min of darkness, while qI takes longer time to recover. Thus, the PAM imaging protocol was modified to include 30-min dark periods, over which recovery of F_m was followed with saturating light pulses given once in 5 min (Figure 4A). We selected lesions that had formed just prior to a dark period and extracted kinetics for these areas in all imaged Sha plants (white arrow in Figure 4A). In these lesions, dark recovery of F_m was incomplete as compared with the undamaged leaf areas. This suggested that the initial drop in F_m' was likely associated with PSII damage, and not with the qE component of NPQ (Figure 4A). Moreover, in the lesioned areas F_m continued to decline during the dark period, indicating inhibition of PSII activity. The fact that inhibition occurred in darkness hinted that O_3 exposure triggered programmed light-independent deterioration of photosynthesis.

As a complementary approach, we measured ultra-fast kinetics of ChlF rise (OJIP) in Col, Sha, and Cvi during a 4 h

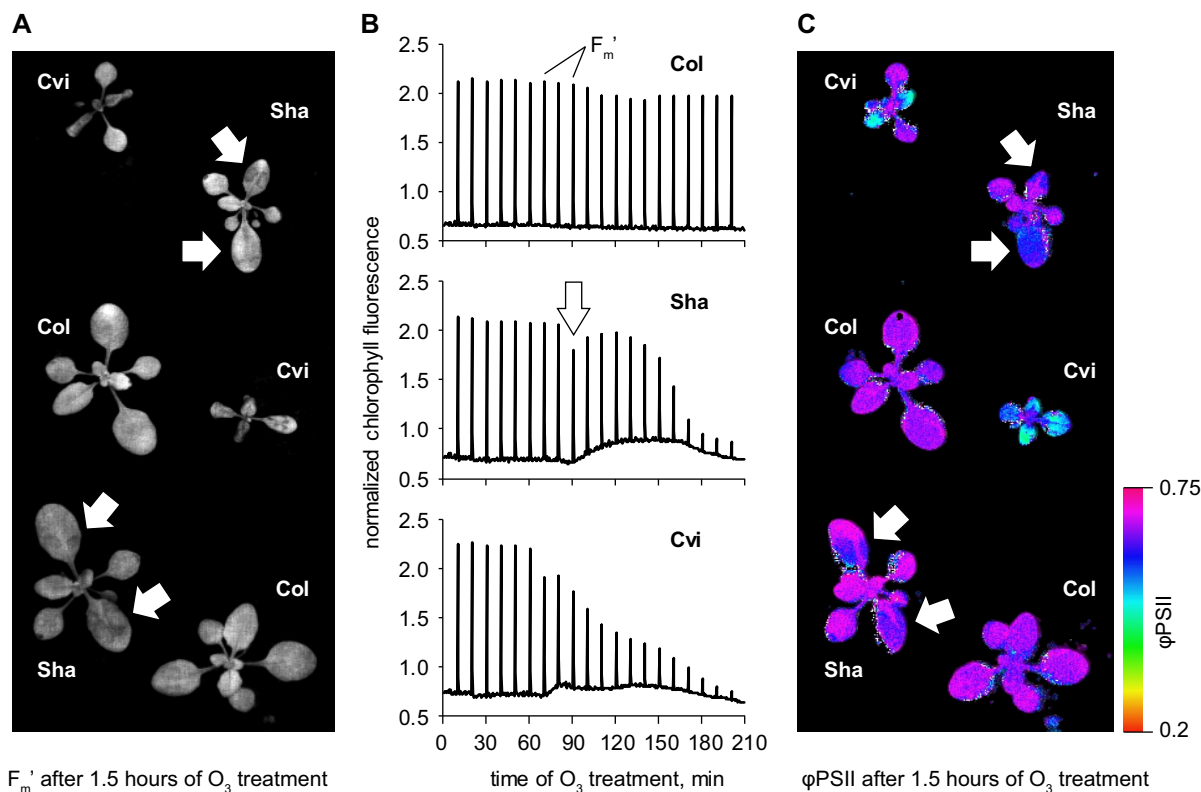


Figure 3 Imaging photosynthesis under O_3 exposure. A, Representative image of O_3 -induced lesions recorded during a saturating light pulse (F_m') with the Imaging PAM. Local lesions characteristic of Sha are labeled with arrows. B, ChlF kinetics extracted from the PAM imaging experiment shown in (A). Saturating light pulses to measure F_m' are labeled. Sha-specific transient depression in F_m' is shown with an arrow. C, Effective quantum yield of $\phi PSII$ in the same experiment as in (A). Arrows indicate local depressions of $\phi PSII$ in Sha.

O_3 exposure (Figure 4B). In essence, this method relies on time-resolved recording of ChlF rise during a saturating light flash. On a logarithmic time axis, this rise reveals inflections F_j and F_i . The rise of fluorescence from F_o to F_j is usually associated with progressive reduction of PSII primary quinone electron acceptor Q_A . The F_j – F_i rise is related to reduction of intersystem electron carriers between PSII and Photosystem I (PSI). Finally, the rise from F_i to F_p ($= F_m$) corresponds to reduction of electron acceptors downstream from PSI such as ferredoxin (Bussotti et al., 2011; Stirbet and Govindjee, 2011, 2012). Only small changes in OJIP kinetics were observed in Col, suggesting little effect of the O_3 treatment on photosynthetic electron transfer. In Cvi, dramatic drop of all OJIP phases was detected over the course of O_3 exposure, while Sha demonstrated intermediate response. Importantly, both in Cvi and Sha the O_3 -induced decrease in fluorescence was observed as early as at the F_o – F_j phase (i.e. within 1 ms of OJIP kinetics; Figure 4B). The effects of the qE component of NPQ on OJIP kinetics are known to develop after several hundred milliseconds of illumination (Antal et al., 2011; Shapiguzov et al., 2019). This supported the idea that the O_3 -induced quenching of ChlF was not associated with qE (Figure 4, A and B).

The shape of OJIP kinetics assessed in O_3 lesions was different between Sha and Cvi (Figure 4C). In Cvi, the decline in F_i – F_m phase occurred faster than in Sha, while the decline

in F_o – F_j was similar in the two accessions. This suggested that Cvi experienced more rapid changes in electron transfer through PSI, than Sha. The parameter $\phi ET2o = 1 - (F_j/F_m)$ depending on both F_j and F_m has been associated with quantum yield of electron transfer from PSII to plastoquinone (Stirbet and Govindjee, 2011; Küpper et al., 2019). O_3 damage lowered $\phi ET2o$ both in Cvi and in Sha, but the effect was more pronounced in Cvi (Figure 4D). Taken together, these results indicated that the inhibitory effect of O_3 on photosynthetic functions was mainly associated with PSII damage, and not with the qE component of NPQ. The different OJIP profiles indicate that inhibition of photosynthesis was occurring through different mechanisms in Sha and Cvi. Overall, the measurements of photosynthesis suggested that O_3 exposure caused programmed decrease of photosynthesis that affected different steps of photosynthetic electron transfer in different accessions.

O_3 triggers unique patterns of gene expression in sensitive Arabidopsis accessions

To gain further insights into mechanisms behind O_3 sensitivity, we monitored O_3 -induced changes in transcriptome in plants exposed to O_3 for 2 h with RNAseq. The Sha data were analyzed together with RNAseq data from Col and Cvi with the same O_3 treatment. Multidimensional scaling plot

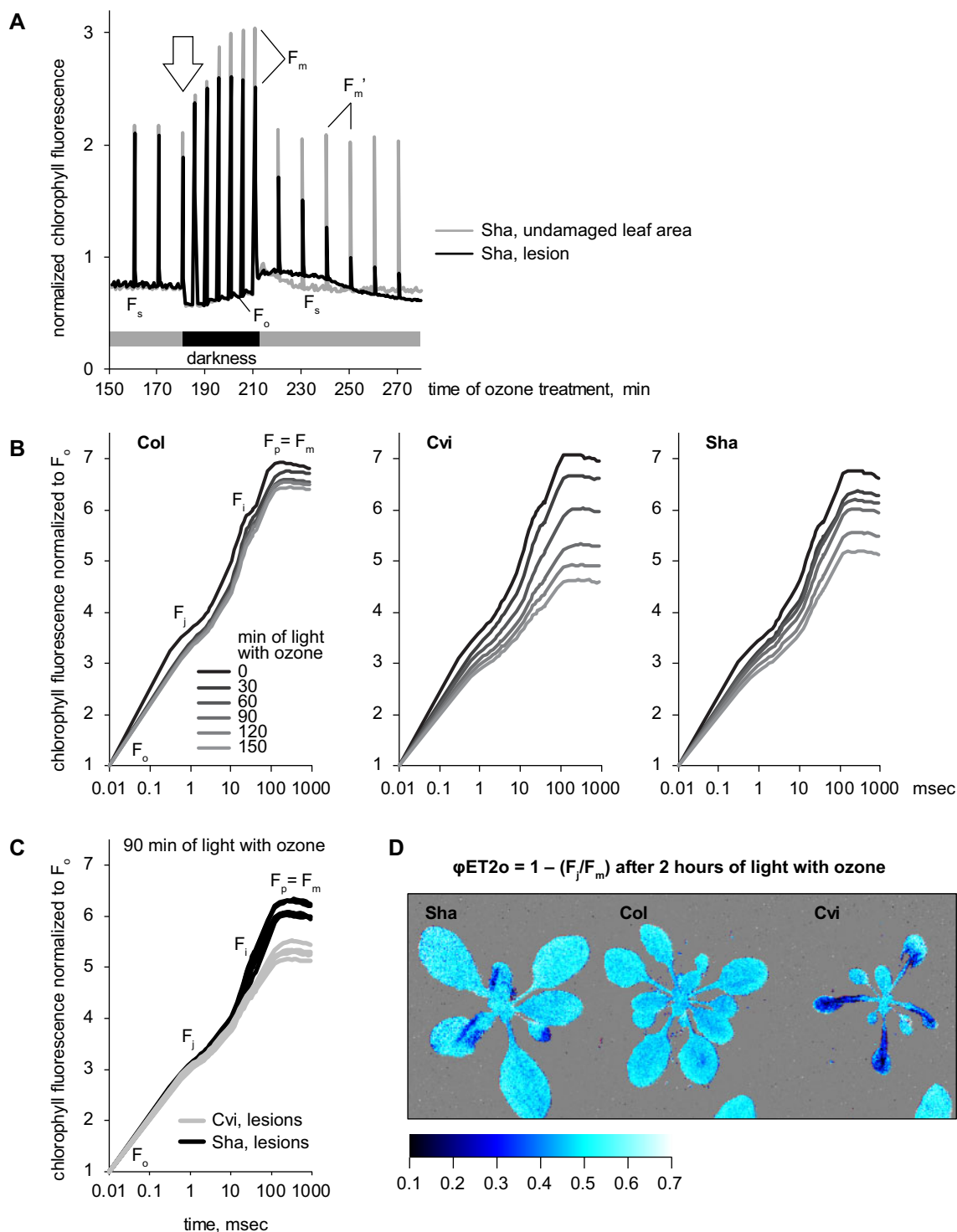


Figure 4 Imaging photosynthesis under O_3 exposure. A, Kinetics of Chf extracted after PAM imaging of O_3 -exposed Sha plants. Maximal fluorescence stimulated with the saturating light pulses in light (F_m') and in darkness (F_m) is indicated. Sha-specific transient drop of F_m' is indicated with an arrow. B, Kinetics of OJIP Chf rise extracted after OJIP imaging of O_3 -exposed plants. The reads are normalized to F_o . Note the logarithmic time axis. C, Comparison of OJIP kinetics recorded in lesioned tissues of Sha and Cvi after 90 min of O_3 exposure. Five representative lesions were selected per each accession. The reads are normalized to F_o . D, False-color image of OJIP parameter $\phi ET2o$ associated with electron transfer from PSII to plastoquinone pool.

of the RNAseq data shows clear separation of gene expression patterns detected for the three genotypes (Figure 5A).

The O_3 effects on transcript levels were determined by performing differential gene expression analysis between

clean air (CA) control and O_3 treatments by genotype. The analysis identified 3,972, 5,243, and 5,099 genes with increased transcript accumulation after 2 h O_3 exposure in Col, Sha, and Cvi, respectively ($FDR \leq 0.05$, $\log_2FC \geq 1.2$;

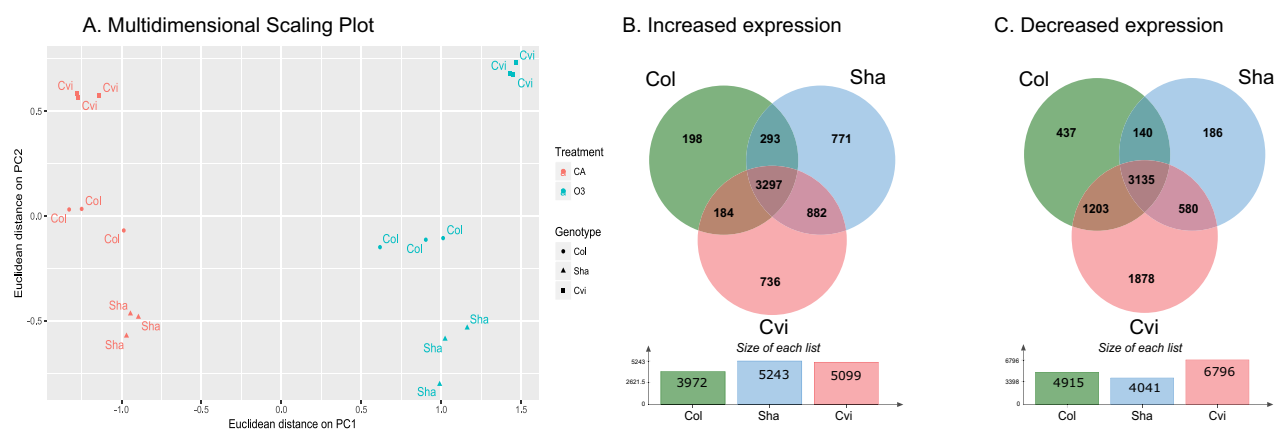


Figure 5 Transcriptional responses induced by O_3 in Col, Sha, and Cvi. The 3.5-week-old plants were exposed to 350 nL L^{-1} of O_3 for 2 h, and changes in transcript accumulation were measured with RNAseq ($n = 3$). A, Multidimensional scaling plot of the data, and (B and C) overlap between genes with increased and decreased expression after the O_3 treatment, respectively.

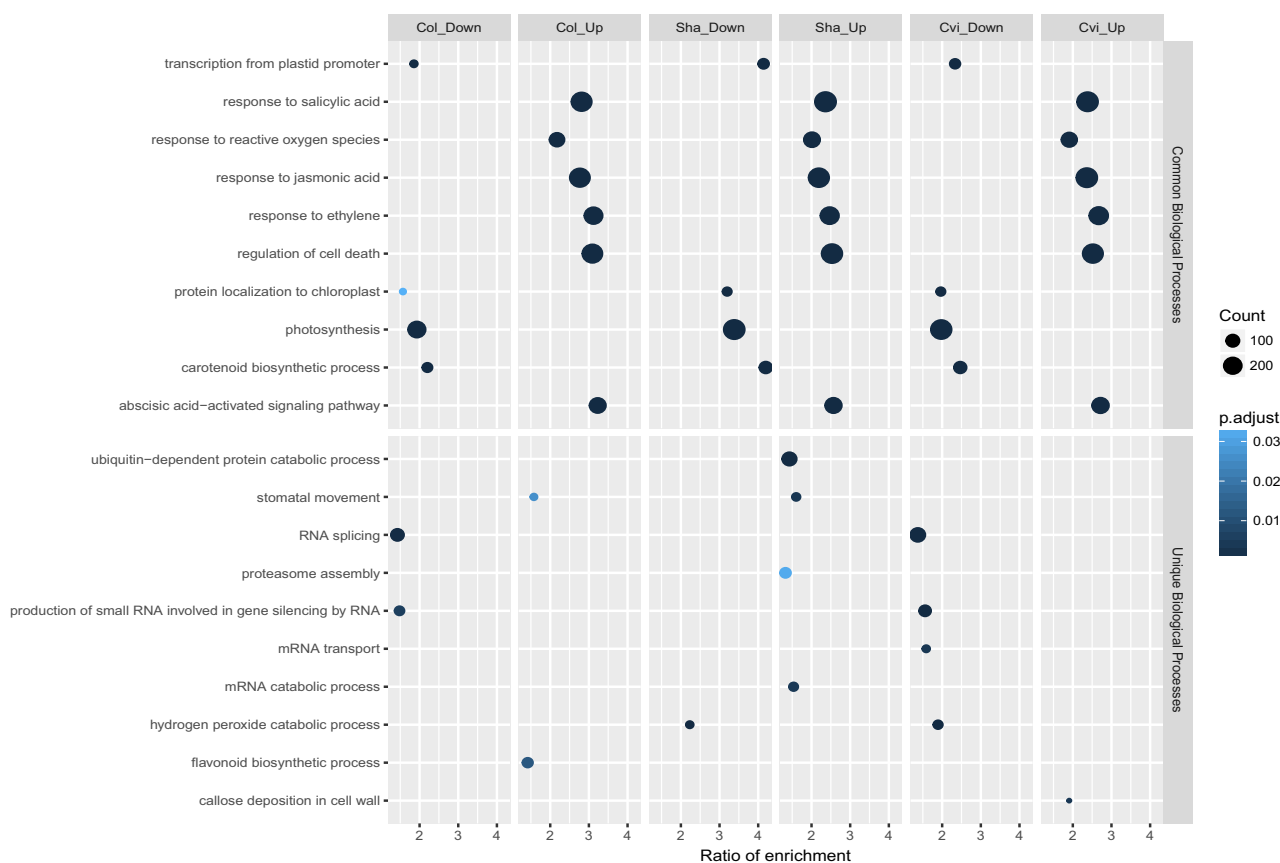


Figure 6 Enrichment analysis of selected GO terms (biological processes) in genes differentially expressed in Col, Sha, and Cvi in response to the O_3 treatment. Ratio of enrichment (proportion of the total genes annotated to a given GO category that are significantly enriched). Count (number of genes).

Figure 5B and Supplemental Table S1). Approximately a half of the genes with increased transcript levels were shared between the three accessions. From the other half, almost 78% of the genes were either unique to Sha or Cvi or shared between them (Figure 5B). O_3 decreased the accumulation of 4,915, 4,041, and 6,796 transcripts in Col, Sha, and Cvi,

respectively ($FDR \leq 0.05$, $\log_2FC \leq 1.2$, Figure 5C and Supplemental Table S1). Nearly 42% of genes with decreased transcript levels were common between the three accessions. In addition, each genotype had unique genes with decreased transcript levels: 437, 186, and 1,878 genes in Col, Sha, and Cvi, respectively (Figure 5, A and C).

A major rationale for studies in *Arabidopsis* is that information gained in this model plant should be informative also for other plant species. We used O₃ transcriptome data from *Medicago* [70 nL L⁻¹, 6 h per day for 6 d (Iyer et al., 2013)] and from rice [108 nL L⁻¹, 7 h per day for 8 d (Ashrafuzzaman et al., 2018)] and compared similarities in O₃ responses between the species. Despite the differences in O₃ treatments, the expression of *Arabidopsis* orthologues induced by O₃ in *Medicago* and rice had 51% and 67% overlap respectively with *Arabidopsis* genes (Supplemental Figure S4A). For genes with decreased expression after O₃, *Medicago* and rice had 62% overlap with *Arabidopsis* (Supplemental Figure S4B).

We next performed gene ontology (GO) enrichment analysis to get further understanding of the physiological processes regulated by genes differentially expressed by the O₃ treatment. Figure 6 shows selected common and unique biological processes regulated by O₃; the complete list of significantly enriched GO terms is provided in Supplemental Table S2. The three accessions shared activation of hormone signaling, for example, response to SA, JA, ethylene, and ABA, regulation of cell death and response to ROS (Figure 6). In relation to chloroplast function, transcript levels decreased for nuclear encoded chloroplast localized proteins, photosynthesis, and carotenoid biosynthesis genes in Col, Sha, and Cvi, respectively (Figure 6). However, the number of genes enriched in these GO categories was higher in Sha than in Cvi and Col. This indicates a greater impact of O₃ on the expression of photosynthesis-related components in Sha (Figure 6; Supplemental Table S2).

For genes responding to O₃ exclusively in Sha and Cvi (Figure 5, B and C), different biological processes were enriched in the two accessions (Figure 6; Supplemental Table S3). Genes annotated to mRNA and protein catabolic processes, fatty acid, and lipid metabolism among others had increased transcript levels only in Sha (Figure 6; Supplemental Table S3). The increased transcript levels for flavonoid biosynthesis genes observed in Col was absent in both O₃-sensitive accessions (Figure 6). In addition, Sha and Cvi had decreased expression levels of genes involved in H₂O₂ catabolism. In agreement with differences in stomatal function previously reported for Cvi and Col (Brosché et al., 2010), Cvi displayed misregulation of genes involved in stomata movements that were otherwise induced by O₃ in Col and Sha (Figure 6; Supplemental Tables S2 and S3).

Regulation of gene expression in response to stress involves multiple signaling pathways and downstream TFs (Xu et al., 2015a). Large-scale experiments have identified the binding sites of many TFs (O'Malley et al., 2016) and curated databases for TFs and binding sites (TF2Network; Kulkarni et al., 2017). We imported the lists of genes differentially expressed into TF2Network, and identified 729 (Col), 682 (Sha), and 684 (Cvi) TFs as potential regulators of genes with increased transcript abundance under O₃ (Supplemental Table S4). The three accessions shared 86% of the TFs identified (Supplemental Table S5). Members of

the TF families WRKY, ERF, MYB, GATA, and CAMTA, which bind promoter elements of O₃-responsive genes (Xu et al., 2015a), were detected as regulators of genes induced by O₃ in Col, Sha, and Cvi (Supplemental Table S5). More than 21% of genes encoding the enriched TFs were themselves induced by O₃: 155 in Col, 180 in Sha, and 181 in Cvi. Out of these, 22, 25, and 21 O₃-responsive TFs were distinctively regulated in Col, Sha, and Cvi, respectively (Supplemental Table S6). Genes encoding regulators of SA signaling (WRKY38) and two members of the NAC (for NAM [No Apical Meristem], ATAF1-2 [Arabidopsis thaliana Transcription Activation Factor1-2], and CUC2 [Cup-Shaped Cotyledon2]) TF family (ANAC04 and ANAC068) were highly induced by O₃ only in Sha (logFC > 3; Supplemental Table S6). The analysis also identified 487 (Col), 417 (Sha), and 480 (Cvi) TFs that bind to promoter elements of genes with decreased transcript accumulation by the O₃ treatment (Supplemental Table S5). Approximately 75% of these TFs were common between the three accessions indicating similar patterns of gene regulation in response to O₃ (Supplemental Table S5). Genes encoding the enriched TFs showed also lower transcript accumulation under the O₃ treatment. Sha had the lowest proportion of TFs downregulated by O₃ (16.5%) as compared with Col (23.2%) and Cvi (27.2%; Supplemental Table S6).

Discussion

Natural variation offers possibilities to investigate stress responses that extend beyond those defined with standard laboratory strains. As a model plant, *Arabidopsis* has been fundamental to understand plant development and stress responses. However, a vast majority of experiments use the accession Col. As Col represents only a limited part of the genetic variation present in *Arabidopsis* (Alonso-Blanco et al., 2016), the use of additional natural *Arabidopsis* accessions allows the discovery of mechanisms involved in stress/O₃ responses. Previously, we associated O₃ sensitivity in Cvi and other *Arabidopsis* accessions with more open stomata leading to high O₃ uptake (Brosché et al., 2010). Similarly, models for predicting plant O₃ damage rely on O₃ uptake rates (Fiscus et al., 2005; Mills et al., 2018). In contrast, here we show that O₃ sensitivity in Sha is not because of increased stomatal conductance or high O₃ uptake (Figure 2). Hence, in Sha other mechanisms contribute to its O₃ sensitivity that is independent from stomatal function. Previous research with AA-deficient mutants (Col background; Conklin et al., 2000) revealed O₃ sensitivity when AA was 1/3 to 1/4 compared with wild-type concentration. It is possible that the lower concentration of AA and dehydroascorbic acid detected in Sha (Supplemental Figure S2) contribute to its O₃ response. However, it is unlikely that AA is the main determinant of Sha O₃ sensitivity given the lack of significant effects of the O₃ treatment on AA levels in both genotypes.

Photosynthesis and chloroplast functions are known O₃ targets in plants (Clyde Hill and Littlefield, 1969; Fiscus et al.,

2005; Bussotti et al., 2011). Our PAM and OJIP measurements revealed that in response to acute O₃ treatments, photosynthesis was robustly maintained in Col, but decreased in sensitive genotypes, which coincided with development of lesions in the leaves. Both in Sha and in Cvi, O₃-induced lesions were associated with decreased maximal ChlF in light and darkness (F_m' and F_m , accordingly). This effect has been previously observed, however, in the earlier studies the question whether this was due to the qE or qI component of NPQ, was not fully resolved (Fiscus et al., 2005). Our results indicated that the nature of ChlF decreased in Sha and Cvi was not related to energy-dependent NPQ (Figures 3, 4). OJIP imaging suggested that the damage was associated with altered electron transfer through PSI and with decreased quantum yield of electron transfer from PSII to plastoquinone. Interestingly, repression of photosynthesis developed in different ways in Sha and Cvi. Importantly, O₃-induced decay of photosynthetic functions continued in darkness. Light-independent PSII damage has previously been associated with heat stress and over-reduction of plastoquinone pool (Marutani et al., 2012). Our results suggest that similar effects may occur in Sha in response to O₃. In maize (*Zea mays* L.), the effect of O₃ on photosynthesis was dependent on genotype, that is, it is a heritable trait, and improved photosynthesis is a possible target in breeding for O₃ tolerance (Ainsworth, 2017; Choquette et al., 2019). Our results in Cvi and Sha refine the direct target of O₃ in photosynthesis and can help design new screens for O₃ tolerance. Previous studies have also indicated the potential for combining phenotyping methods using ChlF with high-throughput genotyping methods as a promising approach for elucidating the basis for O₃ tolerance in sensitive crops (Ainsworth et al., 2014). As photosynthesis can be monitored in vivo with high space and time resolution, we propose that our photosynthetic measurements could be useful in large-scale phenotyping and breeding programs.

The O₃ treatments used in Arabidopsis typically include higher doses and shorter exposure times than those used in crop species; however, even if experiments with Arabidopsis use relatively high levels of O₃, they are still relevant to understand plant O₃ responses at lower doses. The O₃ transcriptional responses determined in this study had >50% overlap with O₃ regulated genes in Medicago (Iyer et al., 2013) and rice (Ashrafuzzaman et al., 2018; Supplemental Figure S4). Furthermore, mechanisms first identified with high O₃ treatments in Arabidopsis have been key to understand plant defenses at lower doses in other plant species, for example, the identification of AA-deficient Arabidopsis mutants (Conklin et al., 2000).

In addition to the large overlap in O₃-regulated transcripts between accessions, we also show accession-specific responses (Figures 5 and 6; Supplemental Tables S1–S6). Our data indicate that impaired regulation of genes involved in flavonoid biosynthesis and ROS metabolism may

contribute to O₃ sensitivity in Sha and Cvi. Furthermore, O₃ sensitivity in Sha could be mediated by additional mechanisms that involve transcriptional regulation of genes with catalytic functions (Figure 6; Supplemental Table S2). These differences in gene expression between Sha and Cvi under O₃ further indicate that O₃ sensitivity in Arabidopsis is controlled by multiple mechanisms at the level of transcription. One mechanism could involve the activation of different TFs as indicated in our data (Supplemental Table S6). We identified candidate regulators of genes responding in Sha and Cvi, some of them being highly induced by the O₃ treatment. Future studies exploring the roles of these TFs in O₃ responses will help to understand O₃ sensitivity and ROS signaling in plants.

In response to changes in the environment, plants activate signaling pathways to alter transcriptional responses. Application of a chemical that inhibits RNA polymerase II leads to a reduction of O₃-induced cell death (Overmyer et al., 2005). This directly demonstrates that altered transcription is an important aspect of plant responses to O₃. The breakdown of O₃ in the apoplast to various ROS activates the plant enzymatic machinery for further ROS production (Wohlgemuth et al., 2002; Ainsworth, 2017). Active production of apoplastic ROS is triggered by several stresses and is a prominent feature in the defense against pathogens (Qi et al., 2017). Accordingly, there is a large overlap in pathogen- and O₃-regulated transcriptional changes (Vaahtera et al., 2013; Xu et al., 2015a; Vuorinen et al., 2020). In agreement with these previous studies, we report in the three accessions the O₃-induced expression of genes involved in defense response to pathogens including fungus and bacteria, to wounding and to several abiotic stresses such as drought, heat and high light (Supplemental Table S2). The ROS burst produced under many stresses could also, at least partially, explain the phenomenon of cross-tolerance, where treatment with one stress confers tolerance to other stresses (Perez and Brown, 2014). For example, pretreatment with O₃ confers tolerance to virus infection (Sudhakar et al., 2007). Thus, the identification of mechanisms regulating plant O₃ responses has broad implications for understanding plant defense responses, which go beyond the role of O₃ as an air pollutant.

In summary, our study reinforces the importance of genetic variation as a tool to unravel molecular mechanisms of plant responses to O₃. We show that these reactions are complex and mediated by multiple mechanisms, as different O₃-sensitive accessions display different molecular and physiological responses to O₃. Furthermore, our data demonstrate that mechanisms independent of stomatal conductance are also key in these processes. Our findings set a framework for future studies aiming at characterizing molecular and physiological mechanisms allowing plants to respond to high O₃ levels in the atmosphere as a result of high air pollution and climate change.

Materials and methods

Plant material and growth conditions

Seeds of the *Arabidopsis* (*A. thaliana*) accessions Col, Sha, and Cvi were obtained from Nottingham Arabidopsis Stock Center. Seeds of all genotypes used in the experiments were harvested from plants grown under the same conditions. Seeds were sown on 1:1 peat/vermiculite, stratified for 3 d, and then grown at 22/19°C (day/night) for a week. For cell death and transcript accumulation measurements, four geminated seedlings were transplanted into 8 × 8 cm² pots containing fresh 1:1 peat/vermiculite mixture. For photosynthesis measurements, plants were transplanted to a tray containing six pots. Subsequently, plants were grown in controlled environment chambers (Weiss Bio1300; Weiss Gallenkamp) under short day conditions (12/12 h d/night photoperiod) with 250 μmol m⁻² s⁻¹ irradiance at 22°C/18°C (day/night) and 70%/90% relative humidity. All plants were grown under the same conditions until they were used for the experiments. Plants used for gas-exchange experiments were grown as previously described (Kollist et al., 2007).

O₃ treatments and cell death measurements

Three-week-old Col and Sha plants were exposed to O₃ (350–423 nL L⁻¹) in parallel with CA controls that consisted of unfiltered ambient air with normal background O₃ concentrations 10–20 nL L⁻¹, which have no effects on plants (Overmyer et al., 2000). The exposure times ranged from 2 to 6 h depending on the measured response.

O₃-induced cell death was quantified in plants exposed to O₃ 200–350 nL L⁻¹ for 6 h. From five to eight individual rosettes per O₃-treated and CA controls were harvested and soaked into 12 mL of Milli-Q water for 18 h. Thereafter, electrolyte leakage was measured with a conductivity meter (Model FE30; Mettler Toledo, Germany). The total electrolyte content was measured after freeze–thawing and data are expressed as percentage of total ions. The experiments were repeated four times.

Stomatal conductance and gas exchange measurements

Steady-state stomatal conductance and photosynthesis rate were measured from Col and Sha plants under controlled conditions with a GFS-3000 gas exchange system (Walz, Effeltrich, Germany) using a whole *Arabidopsis* rosette cuvette. Stomatal conductance was also measured using a Delta-T Device porometer with a clip-on cuvette (Model AP4; www.delta-t.co.uk). For O₃-induced stomatal closure and the diurnal stomatal aperture experiments, gas exchange was monitored with a custom-built gas exchange device, and data analyzed as previously described (Kollist et al., 2007).

Spectroscopic measurements of photosynthesis

Photosynthetic performance was imaged with PAM ChlF imaging (Imaging-PAM, M-series; Heinz Walz, Germany) and a

FluorCam FC 800-C/1010 CUST with Fast Camera TOMI-3 (P.S.I., Czech Republic; Küpper et al., 2019; Shapiguzov et al., 2020). Col, Sha, and Cvi seedlings were transplanted 1 week after germination to a tray containing six pots and grown under 220–250 μmol m⁻² s⁻¹ and a 12/12 h d/night photoperiod for a week. The 2- to 3-week-old plants were treated with O₃ directly inside the imaging devices. Imaging was performed in the morning. For PAM imaging, the minimal (F_o) and maximal (F_m) fluorescences were determined before the lights turned on. Then actinic light (200 μmol m⁻² s⁻¹) was generated by the device light-emitting diode (LED) light sources. O₃ exposure started 1.5 h after the onset of actinic light. Saturating flashes were triggered every 10 min to assess maximal fluorescence under light (F_m'). The effective quantum yield of PSII photochemistry (ϕ PSII) was calculated as ϕ PSII = ($F_m' - F_s$)/ F_m' (Genty et al., 1989). The kinetics of ChlF was normalized to F_o . For the imaging of OJIP (F_o , F_j , F_i , F_p) transients, plants were shifted in the morning from growth light conditions to the imaging system that was pre-equilibrated with O₃ (350 nL L⁻¹). Immediately after the shift, the plants were dark-adapted for 10 min, after which OJIP at time 0 was imaged. Then consecutive 30-min periods of actinic light (200 μmol m⁻² s⁻¹) started, each followed by a 10-min dark adaptation and OJIP imaging. The OJIP imaging protocol included three measurements of the background signal, then three 20-μs flashes of saturating light for F_o measurement and finally a saturating flash (1.2 s of 3,500 μmol m⁻² s⁻¹). During the saturating flash, images were recorded at 0, 0.3, 0.6, 0.9 ... 5.1 ms; 5.4, 7.8, 10.2 ... 101, 4 ms; 102, 132, 162 ... 1,092 ms following the start of the pulse. Three background and three F_o values were averaged.

RNA sequencing

The 3-week-old Col, Sha, and Cvi plants were exposed to O₃ 350 nL L⁻¹ and CA for 2 h. Four rosettes per treatment and genotype were harvested immediately after exposure, snap-frozen in liquid nitrogen and stored at –80°C until analyzed. Total RNA was extracted with TRIzol (Invitrogen). RNA quality was checked with Agilent 2100 Bioanalyzer and the concentration measured with nanodrop ND-1000 (NanoDrop Technologies). RNAseq library preparation and sequencing were performed at the Institute of Biotechnology, University of Helsinki using three biological replicates. Libraries were constructed using TruSeq Standed mRNA Sample PrepKit (Illumina) following manufacturer's instructions. The library concentration was measured using Qubit Fluorometer, and the quality and size were checked by Fragment Analyzer (Advanced Analytical, AATI). Libraries were sequenced on NextSeq 500 (Illumina).

RNAseq data analysis was done in Chipster (Kallio et al., 2011) and in R (R Development Core Team 2018), version 3.5.0. The quality of raw reads was inspected in Chipster with FastQC (Andrews, 2014). Removal of adapter sequences, trimming and cropping of the reads was done using Trimmomatic-0.33 (Bolger et al., 2014) in single-end mode. The bases with a Phred quality score less than 20 were

trimmed from the ends of the reads and reads shorter than 30 bases were removed from the analysis (-phred33, TRAILING:20 and MINLEN:30). Filtered reads were mapped to the Arabidopsis transcript reference database AtRTD2 (Zhang et al., 2017) using Kallisto V-0.43.0 (CMD:quant; Bray et al., 2016) with 4,000 bootstrap sets. The final count table for each biological replicate was obtained as the mean of the bootstrap runs. The count table was used as input to edgeR (v 3.14.0; Robinson et al., 2009) to carry out differential gene expression analysis. Genes with no expression were removed and the filtered count table was normalized using the default Trimmed Mean of *M*-values. The glmLRT method was used to fit the statistical model in edgeR, and Benjamini–Hochberg false-discovery rate correction of *P*-values was used to adjust for multiple testing, with false discovery rate (FDR) ≤ 0.05 as significance threshold.

The overlap between lists of genes differentially expressed genes by O₃ was visualized in jvenn (Bardou et al., 2014). Venn diagrams were also used to compare genes induced by acute O₃ exposure in our study with Arabidopsis orthologues regulated by chronic O₃ exposure in Medicago (Iyer et al., 2013) and in rice (*O. sativa* L; Ashrafuzzaman et al., 2018). Arabidopsis orthologs from Medicago (*M. truncatula*) were reported in (Iyer et al., 2013) and those from rice were obtained from the Rice Genome Annotation Project (http://rice.plantbiology.msu.edu/home_overview.shtml). GO term enrichment was performed using clusterProfiler (Yu et al., 2012). The ratio of enrichment, that is the proportion of the total genes annotated to a given GO category which are significantly enriched in a particular gene set, was calculated by dividing the clusterProfiler estimated parameters gene ratio by the background ratio.

Genes differentially expressed by the O₃ treatment were further analyzed by searching for promoter elements in their promoter regions. Enrichment of promoter elements was implemented in TF2Network including 1,793 curated binding site elements corresponding to 916 TFs (Kulkarni et al., 2017).

AA measurements

The concentrations of total AA and dehydroascorbate were determined spectrophotometrically according to (Gillespie and Ainsworth, 2007). Three-week-old Col and Sha plants were exposed to 350 nL L⁻¹ of O₃ or CA for 2 h. Measurements from fresh leaves were performed immediately after the O₃ treatment.

Statistical analysis

Statistical analysis was performed in R. Linear mixed-effects models with replicates as random-grouping factors were fitted and two-way analysis of variance was calculated using function lme from package 'nlme' (Pinheiro et al., 2018). Function fit.contrast from package gmodels 2.18.1 (Warnes et al., 2018) was used to fit pairwise contrasts defined a priori and *P*-values adjusted with the function p.adjust. Figures were plotted using ggplot2 (Wickham, 2009).

Accession number

RNAseq raw data were deposited at Gene Expression Omnibus with the accession numbers (GSE65740 and GSE117052).

Supplemental data

The following materials are available in the online version of this article.

Supplemental Figure S1. O₃ response in Col and Sha plants treated with two different doses of O₃ for 6 h.

Supplemental Figure S2. Ascorbic acid measurements in Col and Sha plants exposed to 350 nL L⁻¹ O₃ for 2 h.

Supplemental Figure S3. Gas exchange parameters in Col and Sha subjected to O₃ treatments.

Supplemental Figure S4. Identification of common O₃ regulated genes in Arabidopsis, Medicago, and rice.

Supplemental Table S1. List of differentially expressed genes in Col, Sha and Cvi after 2 h O₃ (350 nL L⁻¹) treatment as determined with RNAseq (EdgeR, FDR ≤ 0.05).

Supplemental Table S2. List of significantly enriched GO terms associated to differentially expressed genes (FDR ≤ 0.05).

Supplemental Table S3. List of significantly enriched GO terms associated to O₃ regulated genes exclusively in Sha and Cvi (FDR ≤ 0.05).

Supplemental Table S4. List of transcription factors whose motifs were significantly enriched in the promoter of differentially expressed genes (FDR ≤ 0.05).

Supplemental Table S5. Overlap between TFs predicted to regulate the expression of genes responding to the O₃ treatment.

Supplemental Table S6. Overlap between genes encoding TFs predicted as regulators in the enrichment analysis which were differentially expressed by the O₃ treatment.

Acknowledgments

Tuomas Puukko and Leena Grönholm are acknowledged for technical assistance. We thank Klára Panzarová, Zuzana Benedikty, and Martin Trtílek (P.S.I., Czech Republic) for providing the OJIP imaging FluorCam.

Funding

This work was supported by the Academy of Finland Centre of Excellence in Molecular Biology of Primary Producers (2014–2019, decision 271832 and 307335), Estonian Research Council (grants PRG719 and PRG433) and European Regional Development Fund (Center of Excellence in Molecular Cell Engineering CEMCE).

Conflict of interest statement. None declared.

References

- Ainsworth EA (2017) Understanding and improving global crop response to ozone pollution. *Plant J* **90**: 886–897
- Ainsworth EA, Serbin SP, Skoneczka JA, Townsend PA (2014) Using leaf optical properties to detect ozone effects on foliar biochemistry. *Photosynth Res* **119**: 65–76

- Ainsworth EA, Yendrek CR, Sitth S, Collins WJ, Emberson LD** (2012) The effects of tropospheric ozone on net primary productivity and implications for climate change. *Annu Rev Plant Biol* **63**: 637–661
- Alonso-Blanco C, Andrade J, Becker C, Bemm F, Bergelson J, Borgwardt KMM, Cao J, Chae E, Dezwaan TMM, Ding W, et al.** (2016) 1,135 Genomes reveal the global pattern of polymorphism in *Arabidopsis thaliana*. *Cell* **166**: 481–491
- Andrews S** (2014) FastQC: A quality control tool for high throughput sequence data. Babraham Bioinformatics. <https://www.bioinformatics.babraham.ac.uk/projects/fastqc/> (June 12, 2019)
- Antal TK, Osipov V, Matorin DN, Rubin AB** (2011) Membrane potential is involved in regulation of photosynthetic reactions in the marine diatom *Thalassiosira weissflogii*. *J Photochem Photobiol B Biol* **102**: 169–173
- Ashrafuzzaman M, Haque Z, Ali B, Mathew B, Yu P, Hochholdinger F, de Abreu Neto JB, McGillen MR, Ensikat HJ, Manning WJ, et al.** (2018) Ethylenediurea (EDU) mitigates the negative effects of ozone in rice: insights into its mode of action. *Plant Cell Environ* **41**: 2882–2898
- Atkinson N, Erwin P** (2012) The interaction of plant biotic and abiotic stresses: from genes to the field. *J Exp Bot* **63**: 3523–3544
- Baker NR** (2008) Chlorophyll fluorescence: a probe of photosynthesis in vivo. *Annu Rev Plant Biol* **59**: 89–113
- Bardou P, Mariette J, Escudié F, Djemiel C, Klopp C** (2014) jvarkit: an interactive Venn diagram viewer. *BMC Bioinformatics* **15**: 293
- Blomster T, Salojärvi J, Sipari N, Brosche M, Ahlfors R, Keinänen M, Overmyer K, Kangasjärvi J** (2011) Apoplastic reactive oxygen species transiently decrease auxin signaling and cause stress-induced morphogenic response in *Arabidopsis*. *Plant Physiol* **157**: 1866–1883
- Bolger AM, Lohse M, Usadel B** (2014) Trimmomatic: a flexible trimmer for Illumina sequence data. *Bioinformatics* **30**: 2114–2120
- Brosché M, Merilo E, Mayer F, Pechter P, Puzõrjova I, Brader G, Kangasjärvi J, Kollist H** (2010) Natural variation in ozone sensitivity among *Arabidopsis thaliana* accessions and its relation to stomatal conductance. *Plant Cell Environ* **33**: 914–925
- Bouchabka O, Chang F, Simon M, Voisin R, Pelletier G, Durand-Tardif M** (2008) Natural variation in *Arabidopsis thaliana* as a tool for highlighting differential drought responses. *PLoS One* **3**: e1705
- Bray NL, Pimentel H, Melsted P, Pachter L** (2016) Near-optimal probabilistic RNA-seq quantification. *Nat Biotechnol* **34**: 525–527
- Brosché M, Blomster T, Salojärvi J, Cui F, Sipari N, Leppälä J, Lamminmäki A, Tomai G, Narayanasamy S, Reddy RA, et al.** (2014) Transcriptomics and functional genomics of ROS-induced cell death regulation by RADICAL-INDUCED CELL DEATH1. *PLoS Genet* **10**: e1004112
- Bussotti F, Desotgiu R, Cascio C, Pollastrini M, Gravano E, Gerosa G, Marzuoli R, Nali C, Lorenzini G, Salvatori E, et al.** (2011) Ozone stress in woody plants assessed with chlorophyll a fluorescence. A critical reassessment of existing data. *Environ Exp Bot* **73**: 19–30
- Choquette NE, Ogut F, Wertin TM, Montes CM, Sorgini CA, Morse AM, Brown PJ, Leakey ADB, McIntyre LM, Ainsworth EA** (2019) Uncovering hidden genetic variation in photosynthesis of field-grown maize under ozone pollution. *Glob Chang Biol* **25**: 4327–4338
- Choudhury FK, Rivero RM, Blumwald E, Mittler R** (2017) Reactive oxygen species, abiotic stress and stress combination. *Plant J* **90**: 856–867
- Clyde Hill A, Littlefield N** (1969) Ozone. Effect on apparent photosynthesis, rate of transpiration, and stomatal closure in plants. *Environ Sci Technol* **3**: 52–56
- Conklin PL, Saracco SA, Norris SR, Last, RL** (2000) Identification of ascorbic acid-deficient *Arabidopsis thaliana* mutants. *Genetics* **154**: 847–856
- Fiscus EL, Booker FL, Burkey KO** (2005) Crop responses to ozone: uptake, modes of action, carbon assimilation and partitioning. *Plant Cell Environ* **28**: 997–1011
- Genty B, Briantais JM, Baker NR** (1989) The relationship between the quantum yield of photosynthetic electron transport and quenching of chlorophyll fluorescence. *Biochim Biophys Acta Gen Subj* **990**: 87–92
- Gillespie KM, Ainsworth EA** (2007) Measurement of reduced, oxidized and total ascorbate content in plants. *Nat Protoc* **2**: 871–874
- Hörak H, Sierla M, Töldsepp K, Wang C, Wang YS, Nuhkat M, Valk E, Pechter P, Merilo E, Salojärvi J, et al.** (2016) A dominant mutation in the ht1 kinase uncovers roles of MAP kinases and GHR1 in CO₂-induced stomatal closure. *Plant Cell* **28**: 2493–2509
- Huang H, Ullah F, Zhou DX, Yi M, Zhao Y** (2019) Mechanisms of ROS regulation of plant development and stress responses. *Front Plant Sci* **10**: 800, doi: 10.3389/fpls.2019.00800
- Iyer NJ, Tang Y, Mahalingam R** (2013) Physiological, biochemical and molecular responses to a combination of drought and ozone in *Medicago truncatula*. *Plant Cell Environ* **36**: 706–720
- Jakobson L, Vaahtera L, Töldsepp K, Nuhkat M, Wang C, Wang Y-S, Hörak H, Valk E, Pechter P, Sindarovska Y, et al.** (2016) Natural variation in *Arabidopsis Cvi-0* accession reveals an important role of MPK12 in guard cell CO₂ signaling. *PLOS Biol* **14**: e2000322
- Jaspers P, Kangasjärvi J** (2010) Reactive oxygen species in abiotic stress signaling. *Physiol Plant* **138**: 405–413
- Kalladan R, Lasky JR, Sharma S, Kumar MN, Juenger T, Des Marais DL, Verslues PE** (2019) Natural variation in 9-cis-epoxycarotenoid dioxygenase 3 and ABA accumulation. *Plant Physiol* **179**: 01185.2018
- Kallio MA, Tuimala JT, Hupponen T, Klemelä P, Gentile M, Scheinin I, Koski M, Käki J, Korpelainen EI** (2011) Chipster: User-friendly analysis software for microarray and other high-throughput data. *BMC Genomics* **12**: 507
- Khan SA, Li MZ, Wang SM, Yin HJ** (2018) Revisiting the role of plant transcription factors in the battle against abiotic stress. *Int J Mol Sci* **19**: 1634, doi: 10.3390/ijms19061634
- Kollist T, Moldau H, Rasulov B, Oja V, Rämme H, Hüve K, Jaspers P, Kangasjärvi J, Kollist H** (2007) A novel device detects a rapid ozone-induced transient stomatal closure in intact *Arabidopsis* and its absence in *abi2* mutant. *Physiol Plant* **129**: 796–803
- Kontunen-Soppela S, Parviainen J, Ruhanen H, Brosché M, Keinänen M, Thakur RC, Kolehmainen M, Kangasjärvi J, Oksanen E, Karnosky DF, et al.** (2010a) Gene expression responses of paper birch (*Betula papyrifera*) to elevated CO₂ and O₃ during leaf maturation and senescence. *Environ Pollut* **158**: 959–968
- Kontunen-Soppela S, Riikonen J, Ruhanen H, Brosché M, Somervuo P, Pelttonen P, Kangasjärvi J, Auvinen P, Paulin L, Keinänen M, et al.** (2010b) Differential gene expression in senescing leaves of two silver birch genotypes in response to elevated CO₂ and tropospheric ozone. *Plant Cell Environ* **33**: 1016–1028
- Kulkarni SR, Vanechoutte D, Van de Velde J, Vandepoele K** (2017) TF2Network: predicting transcription factor regulators and gene regulatory networks in *Arabidopsis* using publicly available binding site information. *Nucleic Acids Res* **46**: e31
- Küpper H, Benedikty Z, Morina F, Andresen E, Mishra A, Trtílek M** (2019) Analysis of OJIP chlorophyll fluorescence kinetics and Q A reoxidation kinetics by direct fast imaging 1[OPEN]. *Plant Physiol* **179**: 369–381
- Langebartels C, Wohlgenuth H, Kschieschan S, Grün S, Sandermann H** (2002) Oxidative burst and cell death in ozone-exposed plants. *Plant Physiol Biochem* **40**: 567–575
- Marutani Y, Yamauchi Y, Kimura Y, Mizutani M, Sugimoto Y** (2012) Damage to photosystem II due to heat stress without light-driven electron flow: involvement of enhanced introduction of reducing power into thylakoid membranes. *Planta* **236**: 753–761
- Merilo E, Laanemets K, Hu H, Xue S, Jakobson L, Tulva I, Gonzalez-Guzman M, Rodriguez PL, Schroeder JI, Brosché M, et**

- al. (2013) PYR/RCAR receptors contribute to ozone-, reduced air humidity-, darkness-, and CO₂-induced stomatal regulation. *Plant Physiol* **162**: 1652–1668
- Mills G, Sharps K, Simpson D, Pleijel H, Frei M, Burkey K, Emberson L, Uddling J, Broberg M, Feng Z, et al. (2018) Closing the global ozone yield gap: quantification and cobenefits for multi-stress tolerance. *Glob Chang Biol* **24**: 4869–4893
- O'Malley RC, Huang SC, Song L, Lewsey MG, Bartlett A, Nery JR, Galli M, Gallavotti A, Ecker JR (2016) Cistrome and episcistrome features shape the regulatory DNA landscape. *Cell* **165**: 1280–1292
- Overmyer K, Brosché M, Pellinen R, Kuittinen T, Tuominen H, Ahlfors R, Keinänen M, Saarma M, Scheel D, Kangasjärvi J (2005) Ozone-induced programmed cell death in the Arabidopsis radical-induced cell death1 mutant. *Plant Physiol* **137**: 1092–1104
- Overmyer K, Kollist H, Tuominen H, Betz C, Langebartels C, Wingsle G, Kangasjärvi S, Brader G, Mullineaux P, Kangasjärvi J (2008) Complex phenotypic profiles leading to ozone sensitivity in Arabidopsis thaliana mutants. *Plant Cell Environ* **31**: 1237–1249
- Overmyer K, Tuominen H, Kettunen R, Betz C, Langebartels C, Sandermann H, Kangasjärvi J (2000) Ozone-sensitive Arabidopsis rcd1 mutant reveals opposite roles for ethylene and jasmonate signaling pathways in regulating superoxide-dependent cell death. *Plant Cell* **12**: 1849–1862
- Perez LB, Brown PJ (2014) The role of ROS signaling in cross-tolerance: from model to crop. *Front Plant Sci* **5**: 1–6
- Pinheiro J, Bates D, DebRoy S, Sarkar D, R Core Team (2018) nlme: Linear and Nonlinear Mixed Effects Models. <https://cran.r-project.org/web/packages/nlme/index.html>
- Qi J, Wang J, Gong Z, Zhou JM (2017) Apoplastic ROS signaling in plant immunity. *Curr Opin Plant Biol* **38**: 92–100
- Robinson MD, McCarthy DJ, Smyth GK (2009) edgeR: a Bioconductor package for differential expression analysis of digital gene expression data. *Bioinformatics* **26**: 139–140
- Shapiguzov A, Nikkanen L, Fitzpatrick D, Vainonen JP, Gossens R, Alseekh S, Aarabi F, Tiwari A, Blokhina O, Panzarová K, et al. (2020) Dissecting the interaction of photosynthetic electron transfer with mitochondrial signalling and hypoxic response in the Arabidopsis rcd1 mutant. *Philos Trans R Soc B Biol Sci* **375**: 20190413, doi: 10.1098/rstb.2019.0413
- Shapiguzov A, Vainonen JP, Hunter K, Tossavainen H, Tiwari A, Järvi S, Hellman M, Aarabi F, Alseekh S, Wybouw B, et al. (2019) Arabidopsis RCD1 coordinates chloroplast and mitochondrial functions through interaction with ANAC transcription factors. *Elife* **8**: e43284
- Sharma S, Lin W, Villamor JG, Verslues PE (2013) Divergent low water potential response in Arabidopsis thaliana accessions Landsberg erecta and Shahdara. *Plant Cell Environ* **36**: 994–1008
- Shimada Y, Goda H, Nakamura A, Takatsuto S, Fujioka S, Yoshida S (2003) Organ-specific expression of endogenous brassinosteroid-biosynthetic genes and distribution of endogenous brassinosteroids in Arabidopsis. *Plant Physiol* **131**: 287–297
- Sierla M, Hörak H, Overmyer K, Waszczak C, Yarmolinsky D, Maierhofer T, Vainonen JP, Salojärvi J, Denessiouk K, Laanemets K, et al. (2018) The receptor-like pseudokinase GHR1 is required for stomatal closure. *Plant Cell* **30**: 2813–2837
- Stirbet A, Govindjee (2011) On the relation between the Kautsky effect (chlorophyll a fluorescence induction) and Photosystem II: Basics and applications of the OJIP fluorescence transient. *J Photochem Photobiol B Biol* **104**: 236–257
- Stirbet A, Govindjee (2012) Chlorophyll a fluorescence induction: a personal perspective of the thermal phase, the J-I-P rise. *Photosynth Res* **113**: 15–61
- Sudhakar N, Nagendra-Prasad D, Mohan N, Murugesan K (2007) Induction of systemic resistance in *Lycopersicon esculentum* cv PKM1 (tomato) against Cucumber mosaic virus by using ozone. *J Virol Methods* **139**: 71–77
- Suzuki N, Rivero RM, Shulaev V, Blumwald E, Mittler R (2014) Abiotic and biotic stress combinations. *New Phytol* **203**: 32–43
- Szymańska R, Nowicka B, Gabruk M, Glińska S, Michlewska S, Dłuzewska J, Sawicka A, Kruk J, Laitinen R (2015) Physiological and antioxidant responses of two accessions of Arabidopsis thaliana in different light and temperature conditions. *Physiol Plant* **154**: 194–209
- Tanaka Y, Sugano SS, Shimada T, Hara-Nishimura I (2013) Enhancement of leaf photosynthetic capacity through increased stomatal density in Arabidopsis. *New Phytol* **198**: 757–764
- Tian F, Yang D-C, Meng Y-Q, Gao, Jjin, G (2019) PlantRegMap: charting functional regulatory maps in plants. *Nucleic Acids Res* **48**: D1104–D1113
- Vaahtera L, Brosché M, Wrzaczek M, Kangasjärvi J (2013) Specificity in ROS signaling and transcript signatures. *Antioxid Redox Signal* **21**: 1422–1441
- Vahisalu T, Puzörjova I, Brosché M, Valk E, Lepiku M, Moldau H, Pechter P, Wang YS, Lindgren O, Salojärvi J, et al. (2010) Ozone-triggered rapid stomatal response involves the production of reactive oxygen species, and is controlled by SLAC1 and OST1. *Plant J* **62**: 442–453
- Vainonen JP, Kangasjärvi J (2015) Plant signalling in acute ozone exposure. *Plant Cell Environ* **38**: 240–252
- Vuorinen K, Zamora O, Vaahtera L, Overmyer K, Brosché M (2020) Dissecting contrasts in cell death, hormone, and defense signaling in response to botrytis cinerea and reactive oxygen species. *Mol Plant Microbe Interact* **34**: 75–87
- Warnes GR, Bolker B, Lumley T, Johnson RC (2018) gmodels: Various R programming tools for model fitting version 2.18.1 from CRAN. Retrieved June 12, 2019 from <https://cran.r-project.org/web/packages/gmodels/index.html>
- Waszczak C, Carmody M, Kangasjärvi J (2018) Reactive Oxygen Species in Plant Signaling. *Annu Rev Plant Biol* **69**: 209–236
- Wickham H (2009) Ggplot2: Elegant Graphics for Data Analysis. Springer, Berlin, Germany
- Wittig VE, Ainsworth EA, Long SP (2007) To what extent do current and projected increases in surface ozone affect photosynthesis and stomatal conductance of trees? A meta-analytic review of the last 3 decades of experiments. *Plant Cell Environ* **30**: 1150–1162
- Wohlgemuth H, Mittelstrass K, Kschieschan S, Bender J, Weigel HJ, Overmyer K, Kangasjärvi J, Sandermann H, Langebartels C (2002) Activation of an oxidative burst is a general feature of sensitive plants exposed to the air pollutant ozone. *Plant Cell Environ* **25**: 717–726
- Xu E, Vaahtera L, Brosché M (2015a) Roles of defense hormones in the regulation of ozone-induced changes in gene expression and cell death. *Mol Plant* **8**: 1776–1794
- Xu E, Vaahtera L, Hörak H, Hinch DK, Heyer AG, Brosché M (2015b) Quantitative trait loci mapping and transcriptome analysis reveal candidate genes regulating the response to ozone in Arabidopsis thaliana. *Plant Cell Environ* **38**: 1418–1433
- Yu G, Wang L-G, Han Y, He Q-Y (2012) clusterProfiler: an R package for comparing biological themes among gene clusters. *OMICS* **16**: 284–7
- Zhang R, Calixto CPG, Marquez Y, Venhuizen P, Tzioutziou NA, Guo W, Spensley M, Entizne JC, Lewandowska D, Ten Have S, et al. (2017) A high quality Arabidopsis transcriptome for accurate transcript-level analysis of alternative splicing. *Nucleic Acids Res* **45**: 5061–5073